

Original Article

HIF-1 α change in serum and callus during fracture healing in ovariectomized mice

Wenliang Li, Kejie Wang, Zhiwei Liu, Wenge Ding

Department of Orthopaedics, Third Affiliated Hospital of Suzhou University, Changzhou 213003, China

Received October 25, 2014; Accepted December 22, 2014; Epub January 1, 2015; Published January 15, 2015

Abstract: The purpose was to detect the effects of ovariectomy (OVX) on femoral fracture healing through different angiogenesis and HIF-1 α expression in mice. Thirty-six young female C57 mice were randomized into two groups: OVX and age-matched intact control (CON). The femoral fracture was generated at 3 weeks after OVX or CON. At 2 or 4 weeks after fracture, the femoral fracture area was evaluated healing status by bone mineral density (BMD), callus formation and mineralization and neovascularization in callus, biomechanical analysis, and HIF-1 α tests. OVX mice showed lower BMD as compared with CON mice. Callus geometric microstructural parameters of the femora in OVX mice were significantly lower than CON mice. OVX induced significant changes of biomechanical parameters in the femoral fracture healing area. The callus forming, callus neovascularization and HIF-1 α tests in OVX mice were significantly lower than in CON mice. HIF-1 α results have the positive proportion with osteoporotic fracture healing.

Keywords: HIF-1 α , osteoporosis, fracture healing, ovariectomy

Introduction

Osteoporosis and osteoporosis-associated fractures have become major causes of morbidity and mortality among the elderly [13]. Lots of researcher thought that osteoporosis decrease the fracture healing [12, 22], and they believed that aging OVX and the genetic molecular background of osteoporosis cause delayed healing and impair regeneration. However other researcher found osteoporosis increase the fracture healing [11].

They found that the increase in bone turnover markers after hip fracture surgery and the subsequent decrease reflect increased bone formation and remodeling during the healing process. The role of osteoporosis during fracture healing remains controversial [8]. Commonly, the healing of osteoporotic fractures is thought to be more complex than that of normal fractures [24, 25]. Research into the causes of osteoporotic fractures and their underlying mechanisms is therefore crucial. Postmenopausal osteoporosis is one of the most common forms of osteoporosis, but its effects, if

any, on fracture healing and how it exerts such effects require further verification.

Oxygen homeostasis provides a basis for studies of physiology and intermediary metabolism. Hypoxia-inducible factor-1 α (HIF-1 α), as a major oxygen homeostasis regulator, has attracted increasing attention in recent years. As a vasculogenesis- and growth-related transcription factor, it is considered a key factor in angiogenesis. In addition, increased expression of HIF-1 is an adaptive molecular response to ischemia and hypoxia in the early stages. It can regulate the expression of many downstream genes. During fracture healing, HIF can exert effects by adjusting the expression of vascular endothelial cell growth factor (VEGF), human heme oxygenase 1 (HO-1), and inducible nitric oxide synthase (iNOS) [17]. However, to the best of our knowledge, no study has yet explored the role of HIF-1 α during osteoporotic-fracture healing. Using an ovariectomized (OVX) mouse model, we therefore explored the expression of HIF-1 α in calluses and investigated the correlation of HIF-1 α expression with microvessel density (MVD) in new calluses, in an attempt to elucidate the mechanism of osteoporotic fracture healing.

Materials and methods

Experimental design and grouping

A total of 48 6-week-old B6 male mice weighing 25 g were randomized equally into two groups: an OVX group and a control group (CON). All animals were bred in the SPF Animal Breeding Center of Soochow University, with free access to sterilized pellet feed (Ca: 0.95%, P: 0.67%) and sterilized water. Room temperature was maintained at 22°C and relative humidity at 56%. The light: dark photoperiod cycle was maintained at 12:12 h intervals. Regular ultraviolet disinfection and ventilation were also provided. Animals in the OVX group were anesthetized by intraperitoneal injection with ketamine, and bilateral oophorectomy was performed via two small incisions on either side of the lower back. Animals in the control group received sham surgery. Obvious atrophy of the uterus after surgery provided a marker of successful ovariectomy. Three weeks after surgery, all experimental animals underwent surgery under ketamine anesthesia to establish right femur fractures. All surgical procedures were performed under strict aseptic conditions. After surgery, the mice were returned to their cages and allowed to eat freely. The animals were randomly assigned to two postoperative time points: 2 weeks and 4 weeks. Blood samples were obtained in the morning at each time point for biochemical tests. Six mice were anesthetized with ketamine and sacrificed by exsanguinations through the abdominal aorta. Fractured femur specimens were obtained under a dissecting microscope. The intramedullary nail was removed and the specimens were wrapped in phosphate-buffered saline (PBS)-soaked gauze and stored at -20°C for determination of bone mineral density, micro-computed tomography (μ CT), and biomechanical parameters. A further six mice were perfused with silicone rubber (Microfil) and the fractured femur specimens were fixed and decalcified for the detection of callus MVD. Femur specimens from the other six mice were formalin-fixed, EDTA-decalcified, and then cut in the sagittal plane. The middle portion of the femur was dehydrated, embedded, and sliced for immunohistochemical tests. Finally, six right femora from each subgroup were immediately dissected and preserved in liquid nitrogen to determine the content of HIF-1 α in bone tissue using real-time PCR. The contralateral femurs were used as controls in these experiments.

Fracture modeling

In this study, a classic unilateral femoral fracture model was repeated [2, 20]. After anesthesia with ketamine (80 mg/kg), the mice were put in a supine position, with the surgical site prepared and disinfected. Using an incision near the medial patella of the femoral ligament in the right knee, the skin, subcutaneous tissue, fascia, and joint capsule were cut open, followed by an outward shift of the kneecaps. After the femoral condyle was exposed, an opening was made and the medullary cavity was enlarged. A size-14 needle tip was implanted retrogradely as the intramedullary fixation nail. A transverse fracture of the midshaft of the femur was made using the scissors. The cavity was washed with normal saline, and the incision was sutured. The contralateral femurs were used as controls. All mice recovered from the surgical procedure and were returned to their cages when they appeared fully active. They had free access to standard laboratory pellet diet and water and were allowed to move freely. Mice with any marked dislocation of the intramedullary nail or with fractures that were not transverse or at the midshaft were excluded from further analysis.

Measurement of BMD

Femur specimens were thawed and rewarmed at room temperature. Bone density of the femoral fracture area was measured by dual energy X-ray absorptiometry (Hologic QDR 4500), using software ((Hologic QDR Software for Windows XP version, Copyright© 1986-2002 Hologic Inc.) specifically designed for small animals. The same measurement was performed at the corresponding site in the contralateral femur. The measurement for each specimen was repeated three times, and the intra- and inter-group coefficients of variation were < 2%.

Determination of callus formation and mineralization using μ CT

At 2 and 4 weeks after surgery, the microstructures of specimens were determined using μ CT. The voxel was set to 21 μ m. A three-dimensional mineralized callus was obtained based on reasonable mineralized domain values. We defined the fracture callus mineralization threshold (295 mg HA/cm³) as 50% of mineralization, based on previous studies of bone healing [28], and the total callus volume (TV), callus

HIF-1 α and fracture healing

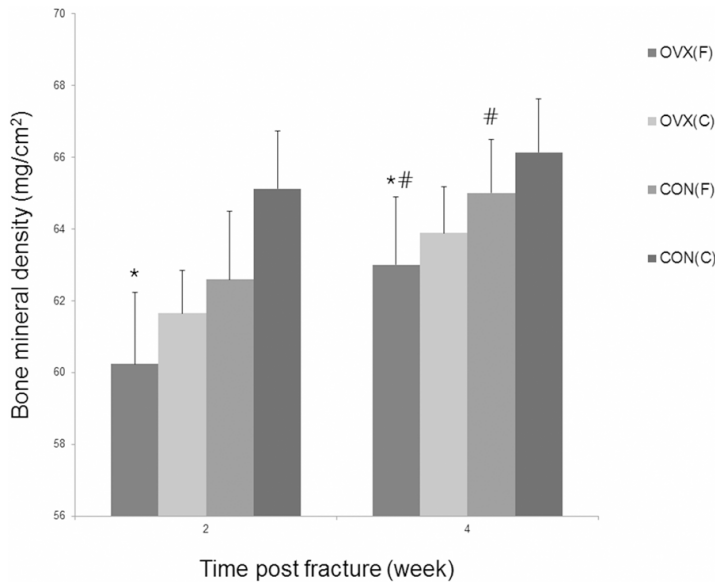


Figure 1. Analysis of Bone mineral density in OVX and CON mice. OVX (F): in fracture healing area in OVX mice; OVX (C): in contralateral limb area in OVX mice; CON (F): in fracture healing area in CON mice; CON (C): in contralateral limb area in CON mice; * $P < 0.05$ vs. CON group, # < 0.05 vs. 2 week.

mineralized volume fraction (BV/TV), and average mineralization density (AMD) were then obtained.

Biomechanics

At 2 and 4 weeks after surgery, the biomechanical properties of the fractured and contralateral femurs were tested. Before biomechanical testing, the specimens were thawed in PBS at room temperature for 3 hours, during which bone mineral density determination and μ CT could be performed. The mechanical characteristics of the femurs were tested using the three-point bending method, with a sample spacing of 10 mm and loading rate of 10 mm/min. Finally, the computer automatically computed the load and final energy, and the internal data (e.g., the final pressure and coefficient of elasticity) were obtained after standardization. The mechanical parameters at the corresponding sites in the contra-lateral femurs were also tested at the same time. The coefficient of variation was $< 5\%$ in this study.

μ CT analysis of callus microvascular status at the fracture site [9]

Mice were placed in a supine position under anesthesia. After routine disinfection, a longitudinal incision was made on the chest. The junction between the left ribs and sternum was

divided to expose the heart. A blunt-ended hollow gauge-7 needle was placed into the left ventricle and fixed. All perfusion fluids were administered through the hollow needle. First, 100 ml heparinized solution was infused to inhibit clotting and promote vasodilation. Blood-letting was performed at the opening of the right atrium to form a circulation path. Silicone rubber (100 ml; Microfil, USA) was infused until the extremities turned yellow and an outflow of silicone rubber in a tiny incision could be observed. After perfusion was completed, the specimens were stored in a 4°C refrigerator overnight to allowing full interaction between the silicone rubber and the specimens. After 24 h, the femurs were taken out of the refrigerator and thawed. The intramedullary nail was removed and the specimen was formalin-fixed, decalcified, and

then placed in 10% formalin for μ CT. The voxel was set at 10.5. Two-dimensional 2D images were initially obtained by μ CT, and then after the volume of interest was obtained, 3D images were also obtained. These 3D images were used to assess vascular volume, volume fraction, and average diameter of the blood vessels.

HIF-1 α levels in serum

Blood samples were centrifuged at 4°C at 2,000 rpm for 10 min to separate the serum. HIF-1 α levels were determined using enzyme-linked immunosorbent assays (Stroughton, MA, USA). The coefficient of variation was $< 10\%$ in our laboratory.

Immunohistochemistry and quantification of HIF-1 α

Femur specimens were fixed in 10% formalin and dehydrated and embedded routinely. Serial sections of 3-4- μ m thickness were sliced from each specimen for immunohistochemical staining (S-P method). An HIF-1 α polyclonal antibody reagent kit was purchased from Santa Cruz. The antibody working dilution was 1:100, and HIF-1 α antigen retrieval was performed by microwave treatment. Serial slice images were obtained using an Olympus microscope attached to a Nikon camera. Positive staining

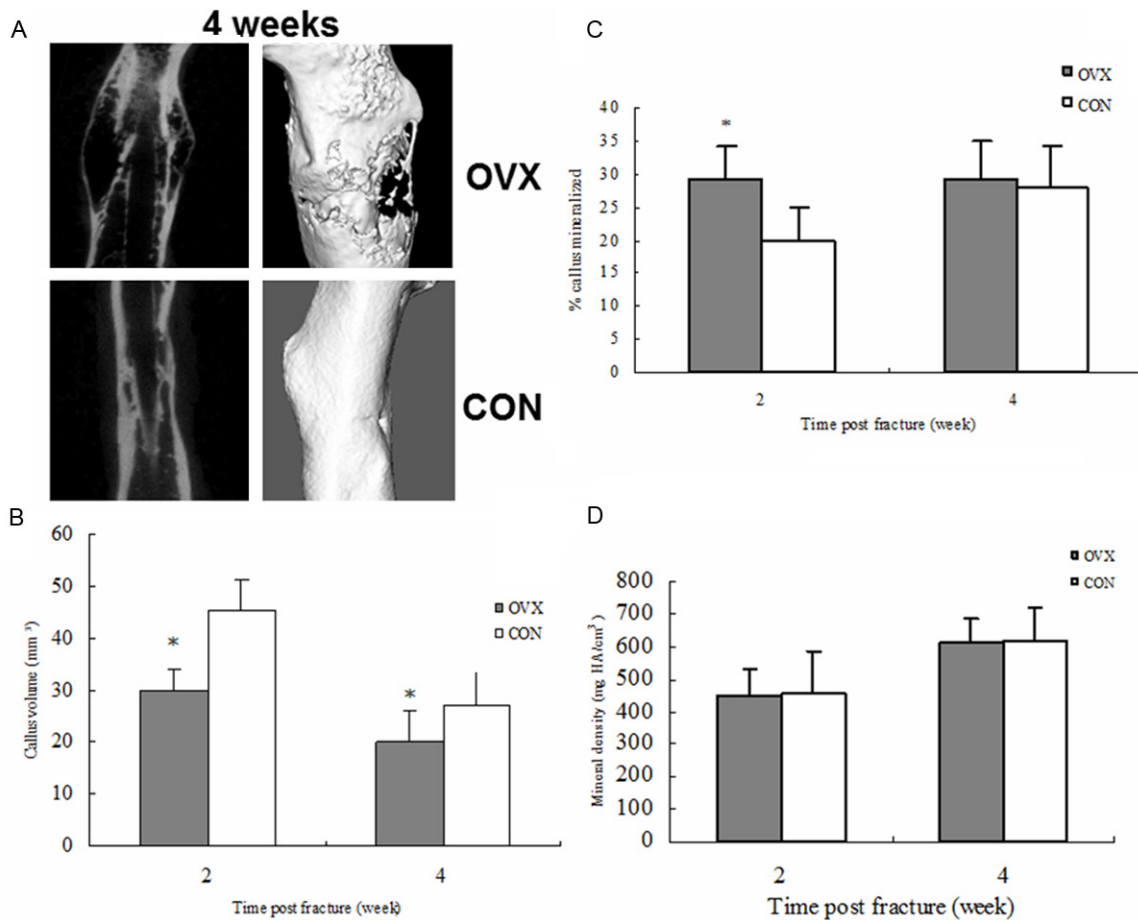


Figure 2. Analysis of bone microarchitecture in fracture healing area with micro-CT in OVX and CON mice. A: 2D tomograms and 3D images of femoral fracture healing area at 4 weeks in OVX and CON mice; B: Callus volume in micro-CT analysis of femoral fracture healing area in OVX and CON mice; C: % callus mineralized in micro-CT analysis of femoral fracture healing area in OVX and CON mice; D: Mineral density in micro-CT analysis of femoral fracture healing area in OVX and CON mice; * $P < 0.05$ vs. CON group.

of HIF-1 α in the callus was indicated by brown spots or wispy bands around the bone marrow, periosteum, and trabecular bone. Spinal cord tissue was used as a positive control and slices without primary antibody served as negative controls. Image Pro Plus (Media Cybernetics, Baltimore, MD) was used to quantitatively analyze the expression of HIF-1 α by calculating the integrated optical density (IOD), which was the sum of pixels in the scanned area in 400 \times higher power images [23]. Intensity was the sum of number of pixels. In the present study, the scattering values of chromogens were determined, which were the complete opposites of the standard values, and high IOD values suggested weak staining [23].

Real-time PCR

Fracture callus tissues were harvested at the designated time points after fracture. Primers

were designed using the Primer 5.0 Express software (F: 5' GCCTTCCTTCTTGGGT 3' and 5' GCATAGAGGTCTTTACGG 3'). SYBR Green intercalating dye (Molecular Probes) was used to perform real time PCR using the Gene Amp PCR System 9700 (Applied Biosystems). After cleaning all extraneous tissue, the tissue was snap frozen in liquid nitrogen. Through homogenized in QIAzol lysis reagent (Qiagen), purified using a commercial kit (Qiagen) and reverse transcribed into cDNA using the Super Script III First Strand Synthesis System (Invitrogen), cDNA was purified using a kit (Qiagen). Standards for the gene were amplified from cDNA and purified. Standard concentrations were determined using spectrophotometric measurement at 260 nm. Standards were continuously diluted to an appropriate range of concentrations. At last, the amount of target gene in the sample was harvested from the standard curves.

HIF-1 α and fracture healing

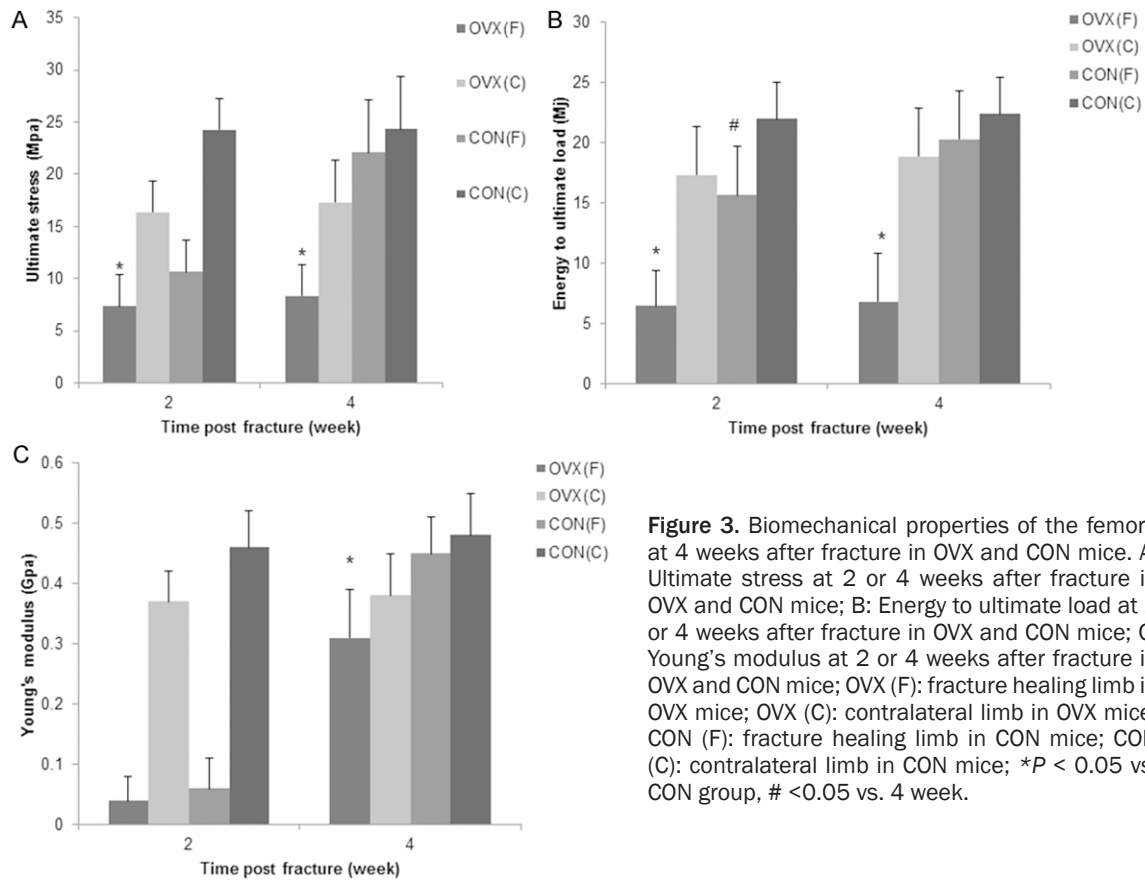


Figure 3. Biomechanical properties of the femora at 4 weeks after fracture in OVX and CON mice. A: Ultimate stress at 2 or 4 weeks after fracture in OVX and CON mice; B: Energy to ultimate load at 2 or 4 weeks after fracture in OVX and CON mice; C: Young's modulus at 2 or 4 weeks after fracture in OVX and CON mice; OVX (F): fracture healing limb in OVX mice; OVX (C): contralateral limb in OVX mice; CON (F): fracture healing limb in CON mice; CON (C): contralateral limb in CON mice; * $P < 0.05$ vs. CON group, # < 0.05 vs. 4 week.

Statistical analysis

Data are presented as mean \pm standard deviations. Two-factor analysis of variance was performed using SPSS 11.5 software, with $P < 0.05$ indicating statistical significance.

Results

General data

During the observation period, two OVX mice died of anesthetic-related complications within 1 day after surgery and were replaced by the same animals. None of the analyzed animals had any obvious complications, and no marked decreases in body weight were seen among the OVX mice.

BMD

Bone densities are shown in the **Figure 1**. Bone density at the fracture-healing areas was significantly lower in the OVX group than in the CON group at 2 and 4 weeks after fracture. Also, the bone density in the middle portion of the femur was higher at postoperative week 4

than at week 2 on both the fractured and the contra-lateral side.

Microstructural changes during fracture healing

Callus volume was significantly smaller in the OVX group compared with the CON group at weeks 2 and 4. The OVX group had a significantly higher mineralization rate at week 2, though the difference was not significant at week 4. Maybe mineralization rate in early stage is different in OVX mice. There was no difference in average density of the callus mineralized area between the groups at either time point (**Figure 2**).

Biomechanics

The results of biomechanical testing are shown in **Figure 3**. At 2 and 4 weeks after fracture, the maximum stress and the maximum load were significantly lower in the OVX group than in the CON group. The energy to maximum load increased significantly from week 2 to week 4 in the CON group, but no such change was found in the OVX group. The elasticity modulus

HIF-1 α and fracture healing

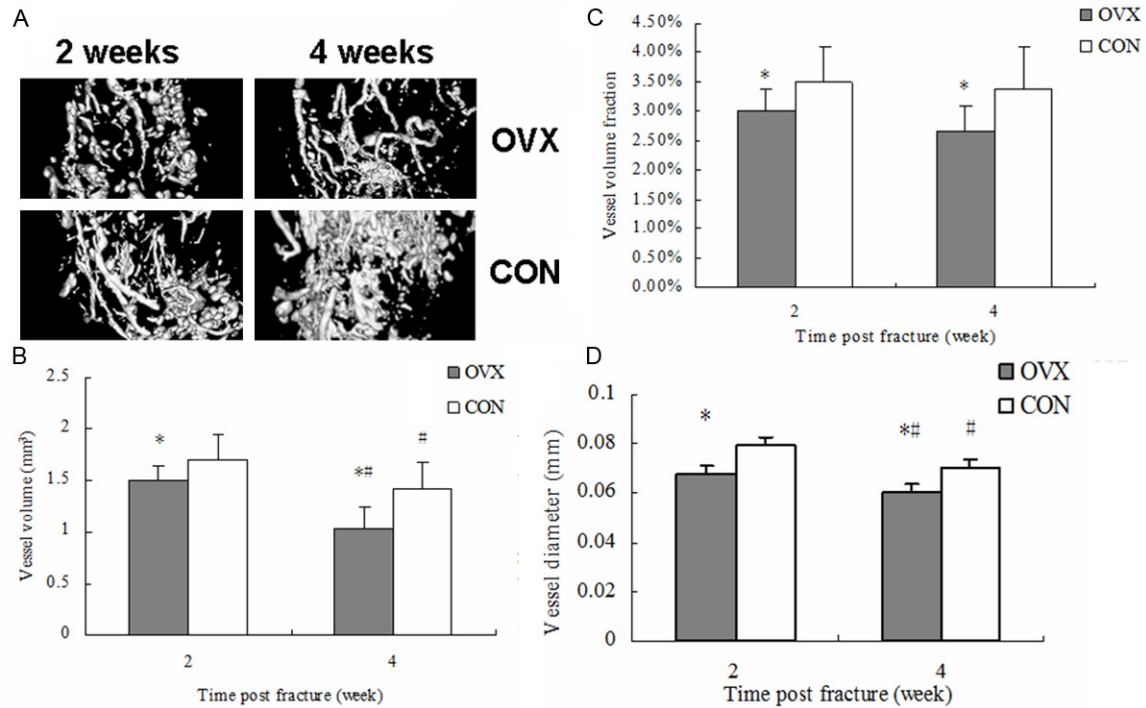


Figure 4. Microvessels of the fracture healing area with micro-CT in OVX and CON mice. A: 2D tomograms and 3D images of femoral fracture healing area in OVX and CON mice; B: Vessel volume in micro-CT analysis of femoral fracture healing area in OVX and CON mice; C: Vessel volume fraction in micro-CT analysis of femoral fracture healing area in OVX and CON mice; D: Vessel diameter in micro-CT analysis of femoral fracture healing area in OVX and CON mice; * $P < 0.05$ vs. CON group, # < 0.05 vs. 2 week.

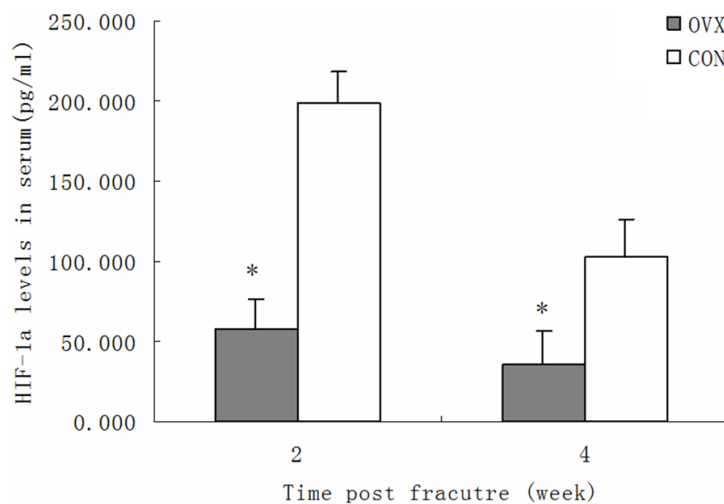


Figure 5. HIF-1 α levels in serum in OVX and CON mice. * $P < 0.05$ vs. CON group.

trast agent-filled and decalcified femur specimens were displayed using μ CT, and the new vessels in the callus were quantified (**Figure 4**). Vascular volume, average vessel diameter, and vascular volume ratio were significantly lower in the OVX group than in the CON group at weeks 2 and 4, and vascular volume and vessel diameter were significantly greater at week 2 than at week 4.

HIF-1 α levels in serum

HIF-1 α levels were slightly lower in the OVX group compared with the CON group at weeks 2 and 4 in serum (**Figure 5**).

was similar in the OVX and CON groups at week 2, but became significantly different at week 4.

Microvessels of callus

To visualize the existing blood vessels surrounding the healing fracture sites, we conducted the Microfill perfusion experiment. The con-

HIF-1 α protein expression

HIF-1 α protein expression at week 4 was seen mainly in the nuclei of vascular endothelial cells, and in part of the cytoplasm, indicated by brown particles (**Figure 6**). In addition, HIF-1 α protein expression was also detected in some loose connective tissue cells around the vascu-

HIF-1 α and fracture healing

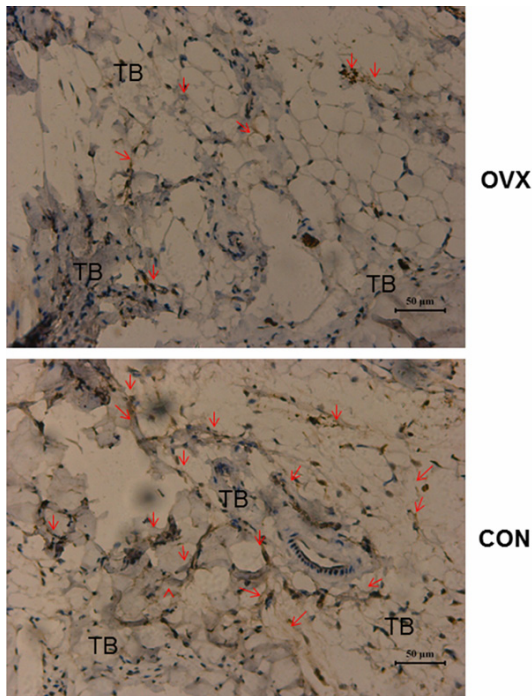


Figure 6. Immunohistochemistry of HIF-1 α in femoral fracture healing area in OVX and CON mice. A: Immunohistochemistry of HIF-1 α in femoral fracture healing area in OVX mice; B: Immunohistochemistry of HIF-1 α in femoral fracture healing area in CON mice; (TB = trabecular bone, Red arrows indicate Hif-1 α immunohistochemistry. Bar = 20 μ m).

lar endothelial cells. HIF-1 α protein expression became even more obvious in areas with accumulated macrophages and fibroblasts. Immunohistochemistry results of HIF-1 α suggested that the IOD (integrated optical density) values in the ovariectomy group were markedly higher than those in the control group (OVX: 62000 \pm 1000, CON: 31000 \pm 3000, $P < 0.05$). Quantitative analysis showed that the immunostained percentage of the bone volume in the ovariectomized mice was also markedly reduced.

Real-time PCR

Quantitative real-time PCR demonstrated the difference of callus HIF-1 α in fractured femora at two time points in all mice (**Figure 7**). The expression of HIF-1 α mRNA was significantly down-regulated in OVX mice in comparison with those in CON group at all time points.

Discussion

The relationship between angiogenesis and bone healing has become a hot research topic

in recent years [5, 19, 21, 29, 31]. Angiogenesis plays an important role in bone development and fracture healing. Research has shown that angiogenic factors, cytokines, stem cells, and progenitor cells can induce bone regeneration and fracture healing [10, 14, 30], among which intracartilage angiogenesis can promote bone repair by increasing blood flow [18]. Angiogenesis thus plays a critical role during bone repair. Our study also demonstrated that HIF, which has angiogenic effects, played a key role during osteoporotic-fracture healing in OVX mice, indirectly indicating that fracture healing is more difficult in OVX mice with osteoporosis than in normal mice.

Bones have mutually anatomized and compensatory vascular networks, which nourish the bone tissue. When a fracture occurs, the blood supply at the fracture site is almost completely interrupted, leading to acute hypoxia and necrosis of the adjacent bone tissues, and a series of resulting pathophysiological changes. Neovascularization in bones is a complex biological process, during which tissue hypoxia plays an important role [27]. HIF-1, with its hypoxia-inducible transcriptional activity, is a specific key regulator of oxygen homeostasis. HIF-1 α is highly sensitive to oxygen concentration, and is therefore known as the “master switch for hypoxic gene expression”. Compared with VEGF, HIF-1 α plays an important role during neovascularization [3, 15, 26]; it can affect fracture healing by regulating angiogenesis and is thus critically important during new bone growth. Some research found new key regulator of the HIF/VEGF axis in osteoblasts in response to hypoxia, critical step for bone angiogenesis [32]. Two aspects of the regulatory effects of HIF-1 on fracture healing have been identified: a) to promote angiogenesis during fracture healing by inducing the expression of pro-angiogenic factors; and b) to regulate directly the functions of bone cells such as osteoblasts, osteoclasts, and chondrocytes. Our current study also confirmed the key role of HIF-1 α during osteoporotic-fracture healing. Levels of HIF-1 α were higher during the early stage of fracture healing compared with the late stage, possibly because tissue hypoxia is more severe in the early stage, which may trigger HIF-1 α production and accelerate fracture healing. We aim to perform further studies to regulate osteoporotic-fracture healing by changing HIF-1 α levels, with important implications for future treatment options for such fractures.

HIF-1 α and fracture healing

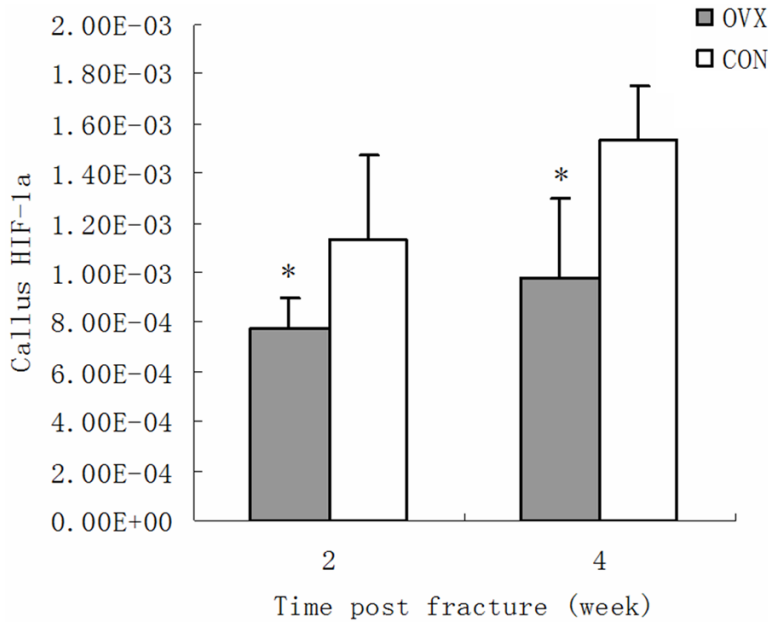


Figure 7. Quantitative real-time PCR of the callus HIF-1 α in fractured femora at two time points in OVX and CON mice. * $P < 0.05$ vs. CON group.

Angiogenesis is important for fracture healing by providing nutrition and various essential osteoblast components. Fracture healing is a complex cell-mediated process. An adequate bone tissue blood supply ensures the provision of the blood cellular components required for fracture repair. Furthermore, pre-osteoblasts, osteoclasts, and chondrocytes in bone marrow participate directly in the whole process of fracture healing after transformation. Wang et al. reported that the coupling of angiogenesis and bone formation can increase the number of osteoblasts and mediate bone formation [31]. Along with angiogenesis, the VEGF/VEGFR2 signaling pathway is considered to increase bone progenitor cells through the outer membrane cells. In the early stage of fracture healing, the microvessels at the periosteum callus have increased activities, while vascular regeneration in the bone can be observed in the late stage of fracture healing. Along with angiogenesis, necrotic tissues and bone debris were removed, followed by the formation and remodeling of the corresponding bone. Fracture induces the involvement of a variety of cells and factors in the complex new bone formation.

Currently, BMD is the gold standard in the detection of osteoporosis and prediction of bone strength. However, BMD does not represent bone structure [6]. The detection of micro-

architecture is also a good way to precisely predict bone strength [4, 16]. Bone strength in the ovariectomized mice was dramatically reduced compared with that in the control group, suggesting impaired integrity of the bone structure, which is consistent with the results from BMD measurement and μ CT. Therefore, the findings of BMD measurement, μ CT, and detection of microarchitecture supported the use of ovariectomized mice as an adequate model of osteoporosis. Nine-week-old mice were used in the present study because osteoporosis and bone resorption were active in these mice, making them susceptible to response to inadequate levels of estrogen.

This allowed significant changes in a short period.

We used 6-week-old mice in our study as bone formation and resorption are both active at this age, and the mouse fracture model can clearly represent the process of fracture healing [5]. In this model, we can observe formation of blood vessels and new bone within a few weeks after fracture. Silicone perfusion combined with micro-CT is a simple and effective method to evaluate angiogenesis [1, 7, 9], and this method can provide both two- and three-dimensional information on angiogenesis as indirect indication of fracture healing.

In summary, osteoporosis after ovariectomy can inhibit or weaken fracture healing, as confirmed indirectly by the expression of HIF-1 α during this process. In addition, the strong angiogenetic effect in the early stage of fracture healing was reflected by the expression of HIF-1 α . Angiogenesis and HIF-1 α play key roles in osteoporotic-fracture healing. Further studies on the regulation of osteoporotic-fracture healing are therefore warranted to improve clinical practices.

Acknowledgements

This study was supported by the hospital and school of medicine where the authors work. We

have no conflict of interest. We thank Dr. Yan Weihong for helpful comments and sincere encouragement.

Disclosure of conflict of interest

None.

Address correspondence to: Dr. Wenge Ding, Department of Orthopedic Surgery, Third Affiliated Hospital of Suzhou University, 185 Juqian Road, Changzhou 213001, China. E-mail: sineboat@126.com

References

- [1] Bentley MD, Ortiz MC, Ritman EL, Romero JC. The use of microcomputed tomography to study microvasculature in small rodents. *Am J Physiol Regul Integr Comp Physiol* 2002; 282: R1267-1279.
- [2] Bonnarens F, Einhorn TA. Production of a standard closed fracture in laboratory animal bone. *J Orthop Res* 1984; 2: 97-101.
- [3] Chavez JC, LaManna JC. Activation of hypoxia-inducible factor-1 in the rat cerebral cortex after transient global ischemia: potential role of insulin-like growth factor-1. *J Neurosci* 2002; 22: 8922-8931.
- [4] Dempster DW. The contribution of trabecular architecture to cancellous bone quality. *J Bone Miner Res* 2000; 15: 20-23.
- [5] Duvall CL, Taylor WR, Weiss D, Wojtowicz AM, Guldberg RE. Impaired angiogenesis, early callus formation, and late stage remodeling in fracture healing of osteopontin-deficient mice. *J Bone Miner Res* 2007; 22: 286-297.
- [6] Felsenberg D, Boonen S. The bone quality framework: determinants of bone strength and their interrelationships, and implications for osteoporosis management. *Clin Ther* 2005; 27: 1-11.
- [7] Garcia-Sanz A, Rodriguez-Barbero A, Bentley MD, Ritman EL, Romero JC. Three-dimensional microcomputed tomography of renal vasculature in rats. *Hypertension* 1998; 31: 440-444.
- [8] Giannoudis P, Tzioupis C, Almaliki T, Buckley R. Fracture healing in osteoporotic fractures: is it really different? A basic science perspective. *Injury* 2007; 38 Suppl 1: S90-99.
- [9] Guldberg RE, Ballock RT, Boyan BD, Duvall CL, Lin AS, Nagaraja S, Oest M, Phillips J, Porter BD, Robertson G, Taylor WR. Analyzing bone, blood vessels, and biomaterials with microcomputed tomography. *IEEE Eng Med Biol Mag* 2003; 22: 77-83.
- [10] Hisatome T, Yasunaga Y, Yanada S, Tabata Y, Ikada Y, Ochi M. Neovascularization and bone regeneration by implantation of autologous bone marrow mononuclear cells. *Biomaterials* 2005; 26: 4550-4556.
- [11] Ikegami S, Kamimura M, Nakagawa H, Takahara K, Hashidate H, Uchiyama S, Kato H. Comparison in bone turnover markers during early healing of femoral neck fracture and trochanteric fracture in elderly patients. *Orthop Rev (Pavia)* 2009; 1:e21.
- [12] Jakob F, Ebert R, Ignatius A, Matsushita T, Watanabe Y, Groll J, Walles H. Bone tissue engineering in osteoporosis. *Maturitas* 2013; 75: 118-124.
- [13] Johnell O, Kanis JA. An estimate of the worldwide prevalence and disability associated with osteoporotic fractures. *Osteoporos Int* 2006; 17: 1726-1733.
- [14] Kawaguchi H, Nakamura K, Tabata Y, Ikada Y, Aoyama I, Anzai J, Nakamura T, Hiyama Y, Tamura M. Acceleration of fracture healing in nonhuman primates by fibroblast growth factor-2. *J Clin Endocrinol Metab* 2001; 86: 875-880.
- [15] Kelly BD, Hackett SF, Hirota K, Oshima Y, Cai Z, Berg-Dixon S, Rowan A, Yan Z, Campochiaro PA, Semenza GL. Cell type-specific regulation of angiogenic growth factor gene expression and induction of angiogenesis in nonischemic tissue by a constitutively active form of hypoxia-inducible factor 1. *Circ Res* 2003; 93: 1074-1081.
- [16] Kleerekoper M, Villanueva AR, Stanciu J, Rao DS, Parfitt AM. The role of three-dimensional trabecular microstructure in the pathogenesis of vertebral compression fractures. *Calcif Tissue* 1985; 37: 594-597.
- [17] Komatsu DE, Hadjiargyrou M. Activation of the transcription factor HIF-1 and its target genes, VEGF, HO-1, iNOS, during fracture repair. *Bone* 2004; 34: 680-688.
- [18] Kosaki N, Takaishi H, Kamekura S, Kimura T, Okada Y, Minqi L, Amizuka N, Chung UI, Nakamura K, Kawaguchi H, Toyama Y, D'Armiento J. Impaired bone fracture healing in matrix metalloproteinase-13 deficient mice. *Biochem Biophys Res Commun* 2007; 354: 846-851.
- [19] Lu C, Marcucio R, Miclau T. Assessing angiogenesis during fracture healing. *Iowa Orthop J* 2006; 26: 17-26.
- [20] Manigrasso MB, O'Connor JP. Characterization of a closed femur fracture model in mice. *J Orthop Trauma* 2004; 18: 687-695.
- [21] Matsuzaki H, Wohl GR, Novack DV, Lynch JA, Silva MJ. Damaging fatigue loading stimulates increases in periosteal vascularity at sites of bone formation in the rat ulna. *Calcif Tissue Int* 2007; 80: 391-399.
- [22] McCann RM, Colleary G, Geddis C, Clarke SA, Jordan GR, Dickson GR, Marsh D. Effect of os-

HIF-1 α and fracture healing

- teoporosis on bone mineral density and fracture repair in a rat femoral fracture model. *J Orthop Res* 2008; 26: 384-393.
- [23] Mendonca DM, Chimelli L, Martinez AM. Quantitative evidence for neurofilament heavy subunit aggregation in motor neurons of spinal cords of patients with amyotrophic lateral sclerosis. *Braz J Med Biol Res* 2005; 38: 925-933.
- [24] Namkung-Matthai H, Appleyard R, Jansen J, Hao Lin J, Maastricht S, Swain M, Mason RS, Murrell GA, Diwan AD, Diamond T. Osteoporosis influences the early period of fracture healing in a rat osteoporotic model. *Bone* 2001; 28: 80-86.
- [25] Nordin BE, Need AG, Chatterton BE, Horowitz M, Morris HA. The relative contributions of age and years since menopause to postmenopausal bone loss. *J Clin Endocrinol Metab* 1990; 70: 83-88.
- [26] Resar JR, Roguin A, Voner J, Nasir K, Hennebry TA, Miller JM, Ingersoll R, Kasch LM, Semenza GL. Hypoxia-inducible factor 1 α polymorphism and coronary collaterals in patients with ischemic heart disease. *Chest* 2005; 128: 787-791.
- [27] Steinbrech DS, Mehrara BJ, Saadeh PB, Greenwald JA, Spector JA, Gittes GK, Longaker MT. VEGF expression in an osteoblast-like cell line is regulated by a hypoxia response mechanism. *Am J Physiol* 2000; 278: C853-860.
- [28] Street J, Bao M, deGuzman L, Bunting S, Peale FV Jr, Ferrara N, Steinmetz H, Hoeffel J, Cleland JL, Daugherty A, van Bruggen N, Redmond HP, Carano RA, Filvaroff EH. Vascular endothelial growth factor stimulates bone repair by promoting angiogenesis and bone turnover. *Proc Natl Acad Sci U S A* 2002; 99: 9656-9661.
- [29] Towler DA. Vascular biology and bone formation: hints from HIF. *J Clin Invest* 2007; 117: 1477-1480.
- [30] van den Dolder J, Farber E, Spauwen PH, Jansen JA. Bone tissue reconstruction using titanium fiber mesh combined with rat bone marrow stromal cells. *Biomaterials* 2003; 24: 1745-1750.
- [31] Wang Y, Wan C, Deng L, Liu X, Cao X, Gilbert SR, Bouxsein ML, Faugere MC, Goldberg RE, Gerstenfeld LC, Haase VH, Johnson RS, Schipani E, Clemens TL. The hypoxia-inducible factor alpha pathway couples angiogenesis to osteogenesis during skeletal development. *J Clin Invest* 2007; 117: 1616-1626.
- [32] Zhu K, Jiao H, Li S, Cao H, Galson DL, Zhao Z, Zhao X, Lai Y, Fan J, Im HJ, Chen D, Xiao G. ATF4 promotes bone angiogenesis by increasing VEGF expression and release in the bone environment. *J Bone Miner Res* 2013; 28: 1870-84.